



Published in final edited form as:

J Med Chem. 2017 November 22; 60(22): 9239–9250. doi:10.1021/acs.jmedchem.7b01113.

Structure-Based Design and Discovery of New M₂ Receptor Agonists

Inbar Fish^{†,‡,‡,‡}, Anne Stöbel^{‡,‡}, Katrin Eitel^{‡,‡}, Celine Valant[§], Sabine Albold[§], Harald Huebner[‡], Dorothee Möller[‡], Mary J. Clark^{||}, Roger K. Sunahara^{||}, Arthur Christopoulos[§], Brian K. Shoichet^{†,*}, and Peter Gmeiner^{‡,*}

[†]Department of Pharmaceutical Chemistry, University of California, San Francisco, San Francisco, California 94158, United States

[‡]Department of Chemistry and Pharmacy, Medicinal Chemistry, Emil Fischer Center, Friedrich Alexander University, Schuhstraße 19, 91052 Erlangen, Germany

[§]Drug Discovery Biology, Monash Institute of Pharmaceutical Sciences, Monash University, Parkville Victoria 3052, Australia

^{||}Department of Pharmacology, University of California, San Diego, La Jolla, California 92093, United States

[‡]Department of Biochemistry and Molecular Biology, George S. Wise Faculty of Life Sciences, Tel-Aviv University, Ramat Aviv, Israel

Abstract

Muscarinic receptor agonists are characterized by apparently strict restraints on their tertiary or quaternary amine and their distance to an ester or related center. On the basis of the active state crystal structure of the muscarinic M₂ receptor in complex with iperoxo, we explored potential agonists that lacked the highly conserved functionalities of previously known ligands. Using structure-guided pharmacophore design followed by docking, we found two agonists (compounds **3** and **17**), out of 19 docked and synthesized compounds, that fit the receptor well and were predicted to form a hydrogen-bond conserved among known agonists. Structural optimization led to compound **28**, which was 4-fold more potent than its parent **3**. Fortified by the discovery of this new scaffold, we sought a broader range of chemotypes by docking 2.2 million fragments, which revealed another three micromolar agonists unrelated either to **28** or known muscarinics. Even

*Corresponding Authors: For B.S.: phone, 01-415-514-4126; bshoichet@gmail.com. For P.G.: phone, +49 9131 85-29383; fax, +49 9131 85-22585; peter.gmeiner@fau.de.

ORCID

Brian K. Shoichet: 0000-0002-6098-7367

Peter Gmeiner: 0000-0002-4127-197X

#Author Contributions

I.F., A.S., and K.E. contributed equally.

Notes

The authors declare no competing financial interest.

Supporting Information

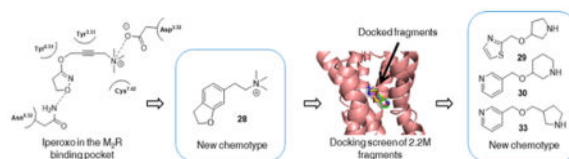
The Supporting Information is available free of charge on the ACS Publications website at DOI: 10.1021/acs.jmed-chem.7b01113.

Docking data, figures of docking poses, functional assay data and experimental procedures, and analytical data of synthesized compounds (PDF)

Molecular formula strings of the target compounds (CSV)

pockets as tightly defined and as deeply studied as that of the muscarinic reveal opportunities for the structure-based design and the discovery of new chemotypes.

Graphical Abstract



INTRODUCTION

With the determination of the atomic resolution structures of ever more G protein-coupled receptors (GPCRs), the question arises of how to exploit them for ligand discovery and design. Although over 30 years of work against soluble proteins have taught a close integration between medicinal chemistry, computation, and structure determination, GPCRs present special challenges. One often wants not only molecules that complement and inhibit a GPCR (inverse agonists), as with enzyme inhibitors, but also agonists that activate the receptors, and the determination of the structures of receptors in their activated states remains rare. Also, most GPCRs have subtypes that recognize identical endogenous agonists but that signal in different organs and that couple to different G proteins, making specificity particularly important and problematic. Finally, structure-based design against GPCRs struggles with the facile determination of cocomplex structures, especially for new ligand series for which affinity is initially weak.^{1,2}

Agonist discovery for the M₂ muscarinic receptor illustrates the opportunities and challenges facing GPCRs. On the one hand, there are compelling therapeutic and chemical-probe arguments for new muscarinic agonists, ideally with new scaffolds. The muscarinic (acetylcholine GPCR) receptors are ubiquitous in human organs, regulating functions ranging from heartbeat to smooth muscle contraction to glandular secretion, to cognition.^{3,4} The receptors are attractive targets for the treatment of conditions like chronic obstructive pulmonary disease, Alzheimer's disease, and overactive bladder syndrome,⁴⁻⁷ and the use of selective muscarinic ligands has recently been discussed for diseases including cancer, diabetes, cardiovascular disease, pain, and inflammation.^{3,8-10} Selectivity is challenging, however, owing to the multiple subtypes with related orthosteric sites signaling in often opposed ways in different organs. Among the five major muscarinic receptor subtypes, the M₁, M₃, and M₅ receptors couple to the G protein G_q, activating phospholipase C, while the M₂ and M₄ subtypes couple to G_i, mediating inhibition of adenylyl cyclase without stimulating PLC, and the differences among the orthosteric sites can be as little as a single amino acid (e.g., the orthosteric sites of the M₂ and M₃ receptors differ only by a Phe → Leu).¹¹⁻¹⁴ This makes other muscarinic subtypes the major off-target for muscarinic drugs. Meanwhile, for agonists, which are wanted to treat diseases like glaucoma, Alzheimer's disease, and Sjögren's syndrome, the design criteria are very tight. Most muscarinic agonists derive from small natural products such as the eponymous muscarine, pilocarpine, and

arecoline, and the activated state crystal structure of the M₂ receptor¹⁵ confirms that the binding site for agonists is highly constrained (Figure 1A).

The restricted agonist site in the M₂ receptor, and the tight chemotypes of even the natural product agonists (Figure 1B–D), suggested a focused search for new agonist scaffolds. Accordingly, we began with complexed conformation of iperoxo bound to the M₂ receptor in its activated state. We initially sought new ligands with an aromatic moiety, substituted with a hydrogen bond acceptor for the interaction with Asn^{6.52} (Ballesteros–Weinstein numbering system¹⁶) and a quaternary amine to ion pair with Asp^{3.32}. This simple strategy succeeded in finding a new scaffold, but to explain the functional effects of the resulting agonists and antagonists, we needed to dock them into the M₂ receptor structures. We used the predicted docking poses to exclude compounds unable to interact with Asn^{6.52}, which we expected would prioritize compounds that can activate the receptor; other contact-based filters, such as interactions with the tyrosines that are an important ligand recognition element in the site, did not add to selectivity among the docking hits. As ever, a primary prioritization criterion was docking scores. Almost all predicted agonists received scores in the range of –27 to –41 kcal/mol, with compounds **25** and **28** only slightly outside that range at –23 and –23.5 kcal/mol. Conversely, all compounds predicted not to be agonists received docking scores higher than (worse than) 0 kcal/mol, except for compound **18** that received a docking score of –15.5 kcal/mol. Whereas docking scores are notoriously inaccurate, this range represents a substantial separation. The resulting model allowed us to prioritize the design of still newer analogues, the most promising of which was a dihydrobenzofuran **28** (Figure 2), which only shares a ECFP4-based Tanimoto coefficients (Tc values) of 0.31 from previous M₂ ligands and appears to be a new scaffold. With this new chemotype defined, we cast a final, broader net, screening a large library for molecules with similar physical properties but greater chemotype diversity. This led to three more agonists in two distinct scaffolds. The hierarchy of approaches used here, beginning with a pharmacophore from the crystallographic conformation of an agonist bound to the active state of the receptor, followed by detailed structural placement, and ending with a large library screen, though inverted from the more typical discovery-and-optimization flow, may be pragmatic for agonist design against other receptors.

RESULTS

Structure-Based Design of New Muscarinic Agonists

The manual design of initial set of 19 compounds depended on the use of a benzene unit as a central scaffold. The aromatic ring was functionalized by a hydrogen bond with Asn^{6.52}-accepting group and a quaternary ammonium salt (to form an ion pair with Asp^{3.32}) that was linked to the aromatic system by various spacers consisting of 1–4 carbons (Figure 2, Table 1). To probe distinct orientations of the functional groups to each other, we synthesized different regioisomers. For some compounds, conformationally restricting elements were installed by bridging either the ammonium salt or the hydrogen bond acceptor group with the benzene scaffold. The analogues included conformationally restricted tertiary and quaternary methoxy or hydroxy substituted aminotetralins. Analogous benzofuran derivatives were also prepared. To fine-tune the distance between the aromatic ring and the

ammonium ion, we synthesized amino-methyl substituted analogues and tetrahydroisochinolines bearing an endocyclic nitrogen atom. Furthermore, we prepared a set of monocyclic derivatives, where the methoxyphenyl and the quaternary ammonium headgroup are linked by a methylene, ethylene, propylene, cyclopropylene, propenylene, or propynylene chain. The methoxy moiety was added either in the ortho- or meta-position of a benzene ring or incorporated into a fused furan. The compounds were synthesized using solution phase chemical reactions including amide coupling, reductive amination, Henry reaction, nucleophilic displacement, reduction of amides and nitroolefins, methylene transfer, or palladium-catalyzed coupling reactions (Supporting Information). Overall, the 19 molecules had Tc values to previously known muscarinic ligands, annotated in ChEMBL and DrugBank, ranging from 0.19 to 0.47.

Structural Complementarity from Docking

All 19 compounds fit the loose pharmacophore described above, but to guide specific structural complementarity, we wanted a more quantitative metric. In parallel with the synthesis, and blind to biological testing, the 19 compounds were docked into the structures of the active and inactive states of the M₂ receptor (PDBs 4MQS¹⁵ and 3UON,¹⁷ respectively). Docking complexes were scored for electrostatic^{18,19} and van der Waals complementarity and corrected for ligand desolvation,^{20,21} and the top scoring configuration of each molecule was retained.

Against the inactive conformation of M₂R, all analogues docked favorably, with energy scores ranging from -38.05 to -45.13 kcal/mol, and all posed to interact with Asp^{3.32} (Supporting Information, Figure S1, Table S1). Conversely, against the active state, only analogues **3** and **17** complemented the more constrained agonist conformation of the orthosteric site, making favorable interactions with Asp^{3.32} and with Asn^{6.52} and scoring well, with scores of -32.89 and -27.79, respectively (Figure 3A and Supporting Information, Figure S1; Table 1). All the other compounds in the first set either scored poorly with unfavorable score, typically above 0 kcal/mol (see above), or did not hydrogen bond with Asn^{6.52}. Superposition of the pose of iperoxo in the active state structure of M₂R with the docked pose of compound **3** (Figure 3B) shows that the tertiary amine of compound **3**, as well as the oxygen forming the hydrogen bond with the Asn^{6.52}, are in the same spatial position as the corresponding moieties of iperoxo.

Binding and Functional Studies at M₁, M₂, and M₃ Muscarinic Receptors

Radioligand binding studies were conducted to evaluate the 19 compounds for their M₁R, M₂R, and M₃R affinity, using [³H]*N*-methyl-scopolamine bromide and membrane preparations from transiently transfected human embryonic kidney cells (HEK).^{22,23} To detect agonists, the ability of the compounds to activate the M₂ receptor was first investigated using a sensitive IP accumulation assay (HTRF detection, IP-One) in HEK cells transiently expressing the human M₂R together with the hybrid G-protein Gα_{qi5HA}.²⁴ Promising compounds were tested in a second, less sensitive but more informative IP accumulation assay in kidney cells from African green monkey (COS) transiently expressing the human M₂R and Gα_{qi5HA}.²⁵ It is the results of this second, higher fidelity assay on which we focus here. The affinity and efficacy profiles of the analogues were compared to

those of the neurotransmitter acetylcholine, the approved drug carbachol, and the superagonist iperoxo (Table 1 and Supporting Information, Table S2).

Compounds **2**, **3** and **5–15** had M_1R , M_2R , and M_3R K_i values in the single- or double-digit micromolar range, and compound **3** had nascent specificity. The conformationally restrained ligands **17–19** had nanomolar K_i values (0.023–0.79 μM). The IP accumulation assay for M_2R activation revealed inverse agonism to strong partial agonism, with E_{max} values ranging from –14% for compound **17** (i.e., inverse agonism) to 75% for compound **3**. Antagonist or very weak agonist effects were observed for the bicyclic compounds **8–17**. While the monocyclic derivatives **5–7**, bearing conformationally restrained moieties, did not substantially stimulate M_2R , the methoxyphenyl compounds **1–3** with the flexible alkylene unit had E_{max} values ranging from 21% to 75% and EC_{50} values in the 10 μM range. These observations agreed broadly with the docking predictions: compound **3** was the most active, compound **17** was among the tightest binding of the 19 ligands, and 16 compounds were correctly classified as antagonists or inverse agonists (Table 1). Admittedly, the docking prioritization was imperfect: compound **1**, which turned out to be a decent agonist, was mispredicted as an antagonist, and compound **17**, notwithstanding its affinity, turned out to be an antagonist.

Structure-Guided Optimization

We sought to optimize for activity by designing a second set of ligands. Two approaches were used: (1) docking of a library of analogues and (2) structure-based design from the docking pose. All nine of the resulting analogues preserve the ethylene linker between the aromatic moiety and the ammonium headgroup of compound **3** that seem important to superpose with iperoxo and well-complement the activated conformation of the M_2R .

In the first approach, a library of 54 analogues was generated and docked against the active state structure. Out of these, four compounds were predicted to be agonists from their ability to hydrogen bond with Asn^{6.52} and their favorable docking scores. These include the secondary amine **20**, the hydroxy analogue **21**, the secondary alcohol **23**, and compound **22** (Table 2 and Supporting Information, Table S1 and Figure S1). On synthesis and testing, compound **22** displayed an improved K_i of 1 μM while retaining specificity over the M_1 and M_3 receptors and substantial agonist activity (Table 2 and Supporting Information, Table S2). Of the other three compounds, the K_i for **20** also improved to micromolar but it lost agonism and specificity, **21** retained activity but was less active than the lead agonist **3**, and **23** lost both affinity and most of its activity. These results, which represent docking failures, are consistent with the idea that while the method can select for fit, both optimization and selection for activation remain challenging it.

In the second approach, which also began with the docking pose, we manually designed and then synthesized analogues of compound **3** by replacing the *meta*-methoxy substituent by an ethoxy, chloro, or trifluoromethoxy group (**25–27**). Additionally, the ketone **24** and the dihydrobenzofuran analogue of compound **17** (compound **28**) were prepared. The conformationally restricted ligand **28** was expected to be a closer surrogate of the lead **3** than the previous unsaturated analogues **17–19** because the electronic properties of the sp^3

oxygen with two lone pairs are more isosteric than the respective sp^2 atom of the benzofuran system. On testing, compound **24** had improved affinity and **25** retained substantial efficacy, but only compound **28**, the conformationally restricted analogue, retained both decent affinity and agonist efficacy for the M_2 receptor in the higher fidelity IP accumulation assay (Table 2 and Supporting Information, Table S2). Overall, the docking prioritized compounds **3** and its phenyl-fluorinated analogue **22**, along with the conformationally restricted **28**, emerged as the most active of the new analogues.

With these results in hand, we decided to more thoroughly investigate **3** and **28** in whole cell assays using Chinese Hamster Ovary (CHO) cells stably expressing the muscarinic receptor subtypes M_1 , M_2 , or M_3 (Table 3, Figure 4). Unlike the assays reported in Tables 1 and 2, these cells recapitulate the native $G_{i/o}$ coupling of the M_2 receptor and the $G_{q/11}$ coupling of the M_1 and M_3 receptors. Whereas the binding affinity and selectivity for compound **3** remained little changed, the apparent affinity of compound **28** improved in the CHO cells to $2 \mu\text{M}$, while its selectivity over M_1 and M_3 receptors improved to 4- and 10-fold, respectively (Table 3 and Figure 4A–C). Looking at $[^{35}\text{S}]\text{GTP}\gamma\text{S}$ binding assay, a classic functional assay for $G_{i/o}$ protein-coupled receptors, **28** was a full agonist with an EC_{50} of $3.3 \mu\text{M}$ and a 100% E_{max} compared to acetylcholine (Figure 4F); compound **3** was also a full agonist in this assay with an EC_{50} only slightly higher at $8 \mu\text{M}$. These values were largely confirmed by a cAMP accumulation assay (Figure 4G). In IP accumulation assays (IP-One assay), which flows from $G_{q/11}$ stimulation through the M_1 and M_3 receptors, both **3** and **28** showed only weak agonist behavior, suggesting specificity for the $M_2\text{R}$, with potencies consistent with their binding affinities (Figure 4D,E), while no IP accumulation was measured via M_2 , as expected given its native $G_{i/o}$ coupling. In a more downstream functional assay, looking at the level of ligand-mediated ERK1/2 phosphorylation, both **3** and **28** behaved as full agonists ($E_{\text{max}} = 100\%$) with potencies of 0.83 and $0.23 \mu\text{M}$ for $M_2\text{R}$ (Figure 4J). Against the M_1 receptor, only **3** had reliable agonist activity, displaying partial agonist profile, while against M_3 neither compound showed substantial activation, suggesting that amplification of signal corresponds with amplification of the new agonists' subtype selectivity (Figure 4I–K). Finally, we determined the ability of **28** to stimulate β -arrestin recruitment via $M_2\text{R}$ activation. Compared to acetylcholine, **28** was a less potent but more efficacious agonist and showed 20-fold bias toward arrestin versus acetylcholine as a reference in the cAMP assay (Table 3, Figure 4H).

These results suggest that compounds **3** and **28** are micromolar to submicromolar full agonists of the M_2 receptor in native signaling, with **28** having moderate arrestin bias versus acetylcholine. The aryl methoxy groups on the “left-hand side” of each molecule represent a new chemotype for the muscarinic receptors, while the distal quaternary nitrogen is well-established. To investigate the replacement of this cationic group and find still newer scaffolds, we turned to large library docking.

Prospective Fragments Library Docking Screen Selection of 10 Compounds

Heartened by the discovery of the new agonists, we sought still more novel agonists from a structure-based screen of a larger chemical library. We screened the “clean fragments” subset of the open access ZINC^{26,27} (<http://zinc15.docking.org>), then just over 2.2 million

commercially available compounds, with $\text{xlogP} = 3.5$, molecular weight = 250 Da, and rotatable bonds = 5, with DOCK3.6.²⁸ Each library molecule was screened in an average of 337.5 orientations in the orthosteric site, and in each orientation an average of 32.6 conformations was sampled. Overall, over 24 billion molecular complexes were evaluated (in a lead-like screen, by comparison, we might evaluate 50-fold more complexes, as the increased molecular size demands more sampling). Configurations were ranked by their electrostatic (using a point charge model of the Poisson–Boltzmann equation, as implemented in QNIFFT)^{29,30} and van der Waals complementarity (using the AMBER potential³¹) to the M_2 active state, corrected for context-dependent ligand desolvation²⁸ (using GB/SA electrostatics implemented in AMSOL^{20,21}), and the top scoring configuration of each molecule was retained. The screen took 37.6 total core hours or less than an hour of elapsed time on our lab cluster.

The result of the calculation was a ranked list of fragments, from most to least complementarity to the M_2 orthosteric active state pocket. The top ranked 1000 (best 0.05%) fragments were inspected for those that interacted with both Asp^{3.32} and Asn^{6.52}. Ten were selected for testing by radioligand displacement and IP accumulation, again using the sensitive (IP-One) and the more informative IP accumulation assay (³H]inositol based) (Table 4, Supporting Information, Table S3). Three of the 10 fragments had micromolar EC_{50} values in the more stringent IP accumulation assay of between 9.9 and 29 μM , and M_2 receptor E_{max} values ranging from 60% to 74% (Table 4, Figure 5). Most of the other fragments had midmicromolar affinities for the M_2R , and several even had substantial agonism in the IP screening assay, but this activity was not retained in the more stringent functional assay (Supporting Information, Table S3). By design, the three new agonists have little similarity to known muscarinic ligands, with ECFP4-based Tc values ranging from 0.20 to 0.34 to annotated ligands in ChEMBL and DrugBank (Table 4). While all three retain the ubiquitous cation of aminergic agonists, the conserved ester/amide of muscarinic agonists has been replaced with either a thiazole (**29**) or a pyridine (**30** and **31**), which has little precedence; in the docked configurations, these heterocycles interact with the same Asn^{6.52} with which the carbonyl system of classic agonists interact. Consistent with the degree of these changes, further alkylation of the aminergic group, which ordinarily would increase activity, for the new agonists diminished it substantially (Table 4 and Supporting Information, Table S3). Structurally, these new agonists represent an even greater departure from known agonist scaffolds than even compounds **3**, **22**, and **28**.

Like many primary neurotransmitters, acetylcholine activates receptors from more than one protein family; such cross-family polypharmacology provides an uniquely chemical organization for signaling.^{32,33} Besides the five muscarinic GPCR subtypes, acetylcholine also activates ligand-gated ion channels as primary targets. These nicotinic acetylcholine receptors (nAChRs) are widely expressed throughout the central and peripheral nervous system and at the neuromuscular junction. Functional nAChRs are a heterogenic group of pentameric ion channels composed of various subunits. Whereas the new docking compounds were chosen for their novelty against known muscarinic ligands, we initially did not consider their similarity to nicotinic ion channel ligands. Unexpectedly, certainly not by design but during the review of this article, we discovered that compounds **3**, **28**, **29**, **30**, **33**,

29a, **30a**, and **33a** had meaningful similarities to known nicotinic ligands, with Tc values ranging from 0.33 to 0.62 (Supporting Information, Table S5). Whereas none were identical to known nicotinic ligands, these similarities are high enough to suggest the new M2 muscarinic agonists might also activate the nicotinic receptor, a cross pharmacology that remains relatively rare, though not completely unknown, outside of acetylcholine itself and its close congeners.

Accordingly, the affinity for the (–)-nicotine binding site at $\alpha 4\beta 2$ nAChR was determined for representative compounds **28**, **30**, and **33**, against the potent radioligand [³H]cytisine. Although all three compounds display nearly identical K_i values for M2 mAChR (11–17 μ M), their affinity for the $\alpha 4\beta 2$ nAChR differs in more than 3 orders of magnitude, resulting in distinct selectivity profiles. While **28** shows equipotent affinities to the muscarinic and nicotinic acetylcholine receptor ($K_i = 9.7 \mu$ M for $\alpha 4\beta 2$ nAChR), the alkyloxymethylpyridines **30** and **33** have pronounced selectivity toward nAChR (K_i values 200 nM for **30** and an extraordinary 1.6 nM for **33**, respectively). Indeed, the affinity of **33** for nAChR resembles the 1.5 nM affinity of nicotine itself. Notably, compounds **30** and **33** share structural similarity with selective $\alpha 4\beta 2$ nAChR ligands of the 3-pyridylether family such as pozaniline (ABT-089, 2-methyl-3-(2-(*S*)-pyrrolidinylmethoxy)pyridine). Pozaniline, epibatidine, and other high affinity $\alpha 4\beta 2$ nAChR (partial-) agonists have been under clinical investigation as cognitive enhancers, including for attention deficit/hyperactivity disorder and Alzheimer's disease, and as analgesics and anxiolytics. Moreover, the $\alpha 4\beta 2$ nAChR partial agonist varenicline is used to effectively enhance smoking cessation. Whereas the functional activity of compounds **30** and **33** is out of scope for this study, such properties may merit future study, as to their role as joint activators of the acetyl cholinergic circuit.

DISCUSSION AND CONCLUSION

Two key observations emerge from this study. First, whereas classical muscarinic agonists reflect a highly constrained pharmacophore, structural complementarity to an activated receptor reveals novel agonists topologically unrelated to those previously known. The modeling that discovered the new agonists suggests that they are recognized via the same interactions made by the classic agonists but using different agonist functional groups. This suggests that there might be many more agonist recognition motifs readily accessible, as neither our pharmacophore-like design nor our library screen pretend to comprehensiveness. Several of these new molecules, like the more optimized **28**, have intriguing signaling properties, including a 20-fold bias toward arrestin signaling vs the endogenous acetylcholine and a signaling specificity for the M₂ vs the M₁ or M₃ receptor subtypes. Second, the new agonists flowed both from a large library docking screen and also from by-hand modeling, the traditional domain of the medicinal chemist. This study supports an alloy between the designing chemist and facile quantitative techniques by which their inspiration can be rapidly checked.

Certain caveats bear mentioning. None of the new agonists have strong activities against muscarinic receptors: none are even at probe levels of activity or specificity, far less than what one would expect from a therapeutic lead, and while novel chemotypes can lead to new

biological effects,^{34–36} the evidence for such here, even with the nascent selectivity and signaling bias of **28**, remains at an early stage. While both the by-hand design and the unbiased molecular docking screen both support the possibility of discovering new agonists for the muscarinic receptors, the docking hits stumbled into chemotypes with high activities against the nicotinic ion channel, against which muscarinic GPCR activity would ordinarily be optimized against (the coactivity against both the ionotropic and metabotropic acetyl choline receptors may itself merit further study).

Still, this study supports a structure-based effort to discover new chemotypes, even in a field as well-ploughed as the muscarinic. We have only undertaken an early reconnaissance into the design of or screens for such agonists; we suspect many more are readily accessible, and a screen of a larger, more elaborated lead-like or drug-like molecules might reveal a broader array of more potent and more selective molecules, as would optimization of the early agonists discovered here. An advantage of these new chemotypes is that by engaging the receptor with new functionalities they can stabilize activated ensembles in manners unexplored by the precedented agonists, engaging effectors in new ways; biased signaling is one example of that. More concretely, they provide templates for the optimization of pharmacokinetic properties that have long been exploited among muscarinic ligands, such as blood–brain penetration, typically defined by tertiary vs quaternary ammoniums. The new agonists, with their new responses to well-established optimization moves, provide new points of departure for medicinal chemistry and probe development programs.

EXPERIMENTAL METHODS

Docking against Active and Inactive State of M₂R

We used DOCK3.6²⁸ to dock molecules against the M₂R active state crystal structure bound to the agonist iperoxo (PDB 4MQS¹⁵) and to the M₂R inactive state bound to QNB (PDB 3UON¹⁷). The same program was used in a docking screen of the “fragments-now” subset of the ZINC database (<http://zinc15.docking.org>). Partial charges from the united-atom AMBER force field were used for all receptor atoms except for Asn^{6,52}, for which the magnitude of the local partial atomic charges were increased to accentuate electrostatic interactions with this particular residue (the net charge of the residue remained neutral), a technique we have widely used previously.^{36,37} Forty-five matching spheres were used. The number of ligand orientations sampled is determined by the values of the bin size, bin size overlap, and distance tolerance, set at 0.3, 0.1, and 1.2 Å, respectively, for both the matching spheres and the docked molecules. The ligand conformations sampled were precalculated using Openeye’s Omega program³⁸ (Openeye Software, Santa Fe NM). Ligand charges and initial solvation energies were calculated using AMSOL (<http://comp.chem.umn.edu/amsol/>).^{20,21}

Ballesteros–Weinstein (BW) Numbering

Receptor residues are referred to by their three-letter code, followed by their Ballesteros–Weinstein (BW) number. In this method, TM residues are identified by a superscript numbering system, in which the residue corresponding to the family A GPCRs most

conserved residue in a given TM is assigned the index X.50, where X is the TM number and the remaining residues are numbered relative to this position.¹⁶

Tanimoto Coefficient (Tc) Calculation

We extracted a data set of 2422 ligands from ChEMBL^{20,39–41} and DrugBank.⁴² Using the GenerateMD program (version 5.10.3) in the Chemaxon package, we calculated the EFCP4 fingerprints which were used to calculate the Tc⁴³ between our hits and all of the 2422 ligands in Table 4.

Membrane-Based Radioligand Binding Experiments

Affinities of the test compounds toward the human M₁, M₂, and M₃ receptors were determined using homogenates of membranes as described previously.^{22,23,44} In brief, HEK293T cells were transiently transfected with the cDNA of the appropriate receptor (purchased from cDNA Resource Center, Bloomsburg, PA) using a solution of linear polyethylenimine in PBS.⁴⁵ Receptor binding experiments were performed in 96-well plates using homogenates of the corresponding receptor together with the radioligand [³H]N-methyl-scopolamine bromide (specific activity of 70 Ci/mmol, PerkinElmer, Rodgau, Germany) at a final concentration of 0.20–0.30 nM for M₁R and M₂R and 0.10–0.20 nM for M₃R at a receptor density (B_{\max}) of 1500 ± 260 , 1400 ± 140 , and 2200 ± 530 fmol/mg, a protein concentration of 3–6, 5–10, and 2–10 $\mu\text{g}/\text{test tube}$, and a K_d value of 0.18 ± 0.052 , 0.20 ± 0.018 , and 0.086 ± 0.005 nM, for M₁R, M₂R, and M₃R, respectively. Unspecific binding was determined in the presence of 10 μM atropine. Protein concentration was established by the method of Lowry using bovine serum albumin as standard.⁴⁶ Resulting competition curves were analyzed by nonlinear regression using the algorithms for one-site competition of PRISM 6.0 (GraphPad, San Diego, CA).

Whole Cell Radioligand Binding Assays

Radioligand binding experiments were performed on CHO-FlpIn whole cells stably expressing the human M₁, M₂, and M₃ receptor constructs of choice. After plating 20000 cells in complete DMEM into 96-well ISOPATE TC plates (all amounts are per well), cells were allowed to grow overnight at 37 °C. The next day, cells were washed with phosphate-buffered saline (100 mL) and resuspended in binding buffer (10 mM HEPES, 100 mM NaCl, 10 mM MgCl₂, pH 7.4). Assay mixtures, in a total volume of 100 μL with a 1/10 dilution of drug, were incubated at room temperature (22 °C) for 6 h. Assays were terminated by buffer removal followed by rapid washing, twice, with ice-cold 0.9% NaCl (100 μL). Plates were allowed to dry inverted for 30 min; OptiPhase Supermix scintillation cocktail (100 μL) was added, plates were sealed (TopSeal), and radioactivity was measured in a MicroBeta2 LumiJET microplate counter. Saturation binding experiments were performed in the absence or presence of atropine (10 μM) with 0.003–3 nM [³H]NMS. Inhibition binding experiments were performed with ~0.2 nM [³H]NMS (the approximate K) in the presence of various concentrations of analogues.

IP Accumulation Assay

For validation of the screening data derived with the IP-One assay (see Supporting Information), the most promising compounds were tested on M₂R activation with an IP accumulation assay as described previously.¹⁵ In brief, COS-7 cells were transiently cotransfected with M₂R and G α_{q153HA} (G α_q protein with the last five amino acids at the C-terminus replaced by the corresponding sequence of G α_i , a gift from The J. David Gladstone Institutes, San Francisco, CA, for which we are grateful) by applying the TransIT-2020 Mirus transfection reagent (MoBiTec, Goettingen, Germany). Eighteen h before, the test cells were incubated with *myo*-[³H]inositol (specific activity = 20.1 Ci/mmol, PerkinElmer, Rodgau, Germany). Test compounds (six different concentrations for each compound, total range from 0.1 pM up to 300 μ M) were incubated for 2 h at 37 °C in triplicate, and resulting radioactivity was measured by scintillation counting. Activation curves were normalized to the maximum effect of carbachol (100%) and buffer (0%) and analyzed using the algorithms for nonlinear regression in PRISM 6.0. For all compounds, 3–8 individual dose–response curves were measured, and the corresponding EC₅₀ and E_{max} values of each mean curve were calculated and summarized to get the average EC₅₀ and E_{max} values \pm SEM.

IP-One Accumulation Assays

The IP-One assay kit (Cisbio, France) was used for the direct quantitative measurement of myoinositol 1-phosphate (IP1) in FlpIn CHO cells stably expressing hM₁ and hM₃ mAChRs. This is a competitive immunoassay that measures the homogeneous time-resolved fluorescence signal transferred between a cryptate-labeled IP1-specific monoclonal antibody and d2-labeled IP1. The fluorescence signal measured is inversely proportional to the concentration of native IP1. Briefly, cells were seeded into 96-well plates at 20000 cells per well and allowed to grow overnight at 37 °C, 5% CO₂. The following day, cells were washed once with PBS then incubated with stimulation buffer (HEPES 10 mM, CaCl₂ 1 mM, MgCl₂ 0.5 mM, KCl 4.2 mM, NaCl 146 mM, glucose 5.5 mM, LiCl 50 mM, pH 7.4) for 60 min at 37 °C, 5% CO₂. Following this incubation, ligands were added at 10 \times their final concentrations (ACh or test compounds) and incubated for a further 40 min prior to terminating the ligand-mediated stimulation by removing the buffer and adding 25 μ L of lysis buffer. Finally, 14 μ L of lysate was transferred into 384-well Optiplate, followed by the addition of 3 μ L of IP1-d₂, then 3 μ L of Ab-Cryp, and incubated for 60 min at room temperature. Time resolved fluorescence resonance energy transfer (HTRF) was determined using the Envision plate reader (PerkinElmer).

[³⁵S]GTP γ S Binding Assay

Membrane homogenates (15 μ g) were equilibrated in a 500 μ L total volume of assay buffer containing 10 mM guanosine 5'-diphosphate and a range of concentrations of ACh or test compounds (1 nM to 100 mM) at 30 °C for 60 min. After this time, 50 μ L of [³⁵S]GTP γ S (1 nM) was added and incubation continued for 30 min at 30 °C. Termination of the reaction and determination of radioactivity were performed by rapid filtration through Whatman GF/B filters using a Brandell cell harvester (Gaithersburg, MD). Filters were washed three times with 3 mL aliquots of ice-cold 0.9% NaCl buffer and dried before the addition of 4 mL of scintillation mixture (Ultima Gold, PerkinElmer Life Sciences). Vials were then left to

stand until the filters became uniformly translucent before radioactivity was determined in dpm using scintillation counting.

cAMP Accumulation Assay

HEK293 cells stably expressing the Epac cAMP sensor,⁴⁷ obtained as a gift from Jesper Mathiesen, were stably transfected with M₂AChR-tetO (a gift from Brian Kobilka). HEK-Epac-M₂tetO cells were grown to confluency and then treated with 2 μg/mL doxycycline and 1 mM sodium butyrate for 40 h to induce expression of the M₂AChR-tetO. Cells were harvested with lifting buffer (0.68 mM EDTA, 150 mM NaCl, 20 mM HEPES, pH 7.4), centrifuged, resuspended in HBSS-HEPES (Hank's Balanced Salt Solution plus 20 mM HEPES, pH 7.4), and pipetted into a 96-well plate (black with clear bottom). After 20 min in the dark at 37 °C, the basal CFP/YFP ratio of the Epac-cAMP FRET sensor was measured at 436 exc and 480/535 ems for 2 min using a SpectraMax M5. Then forskolin (2 μM final), IBMX (1 mM final), and test compound (0–100 μM final) in HBSS-HEPES, pH 7.4, were added and the CFP/YFP ratio area under the curve was measured for 10 min at 37 °C. Basal values were subtracted, and data was analyzed using GraphPad Prism 6.

β-Arrestin Recruitment Assay

HEK293 cells stably expressing tTA dependent luciferase and β-arrestin-TEVprotease were transiently transfected with M₂-TEV-tTA (cells and DNA construct were a gift from Bryan Roth) for measurement of M₂AChR stimulated of β-arrestin recruitment, basically as described at <https://pdspdb.unc.edu/pdspWeb/content/PDSP%20Protocols%20II%202013-03-28.pdf>. The day after transfection, cells were lifted, resuspended in DMEM with 1% FBS, and plated into a poly-D-lysine coated 384-well clear-bottom plate at 15000 cells/well. After at least 6 h, 0–100 μM test compounds in HBSS-HEPES (Hank's Balanced Salt Solution plus 20 mM HEPES, pH 7.4) were added to the cells. The following day, media was replaced with diluted Bright-Glo reagent (Promega, Madison, WI), and after 20 min in the dark, luminescence was measured using a SpectraMax M5. Data was analyzed using GraphPad Prism 6.

ERK1/2 Phosphorylation Assays

These assays were performed using the AlphaScreen-based SureFire kit as described in detail previously.⁴⁸ All data were expressed as a percentage of ERK1/2 phosphorylation mediated by 100 μM of ACh.

Nicotinic Acetylcholine Receptor (nAChR, α4β2-type) Binding Assays

Binding affinities for the three new muscarinic agonists were determined by Eurofins Panlabs, Inc.⁴⁹ Briefly, membranes from human recombinant SH-SY5Y cells with a nAChR expression level of 2000 fmol/mg protein were incubated with the radioligand [³H]cytisine (K_D 0.30 nM) at a concentration of 0.60 nM together with the test compounds (0.1 nM to 300 μM) in binding buffer (50 mM Tris-HCl, pH 7.4) for 120 min at 4 °C. Nonspecific binding was determined in the presence of 10 μM (–)-nicotine. Concentration–response curves were analyzed using MathIQT™ (ID Business Solutions Ltd., UK) to obtain IC₅₀

values by nonlinear, least-squares regression analysis. IC_{50} values were subsequently converted to K_i values using the Cheng and Prusoff equation.⁵⁰

Compound Synthesis and Purity

Compound synthesis and purity is described in the Supporting Information. The purity of all compounds tested was 95% and was confirmed by reverse phase HPLC by applying different elution systems and detecting the UV absorption at two different wavelengths (220 and 254 nm).

Supplementary Material

Refer to Web version on PubMed Central for supplementary material.

Acknowledgments

This work was supported by the U.S. National of Health grants GM106990 and R35GM122481 and by the NHMRC of Australia program grant APP1055134, project grant APP1082318 and by BaCaTeC. C.V. is an Australian Research Council Future Fellow, and A.C. is Senior Principal Research Fellow of the NHMRC.

ABBREVIATIONS USED

Asn	asparagine
Asp	aspartic acid
BW	Ballesteros–Weinstein
CFP	cyan fluorescent protein
CHO	Chinese hamster ovary
COS	kidney cells from african green monkey
DMEM	Dulbecco's Modified Eagle's Medium
ERK	extracellular-signal regulated kinases
FBS	fetal bovine serum
FRET	fluorescence resonance energy transfer
Gαx	G protein α subunit subtype x
GPCR	G protein-coupled receptor
GTPγS	guanosine 5'-O-(thiotriphosphate)
HBSS	Hank's Balanced Salt Solution
HEPES	(4-(2-hydroxyethyl)-1-piperazineethanesulfonic acid
HTRF	homogeneous time-resolved fluorescence
IBMX	3-isobutyl-1-methylxanthine

IP	inositol phosphate
Leu	leucine
Mx	muscarinic Mx receptor
NMS	<i>N</i> -methylscopolamine
nAChRs	nicotinic acetylcholine receptors
Phe	phenylalanine
PLC	phospholipase C
SD	standard deviation
SEM	standard error of mean
Ser	serine
Tc	Tanimoto coefficient
TM	transmembrane
Tyr	tyrosine
YFP	yellow fluorescent protein

References

1. Shoichet BK, Kobilka BK. Structure-Based Drug Screening for G-Protein-Coupled Receptors. *Trends Pharmacol Sci.* 2012; 33:268–272. [PubMed: 22503476]
2. Jazayeri A, Dias JM, Marshall FH. From G Protein-Coupled Receptor Structure Resolution to Rational Drug Design. *J Biol Chem.* 2015; 290:19489–19495. [PubMed: 26100628]
3. Matera C, Tata AM. Pharmacological Approaches to Targeting Muscarinic Acetylcholine Receptors. *Recent Pat CNS Drug Discovery.* 2014; 9:85–100. [PubMed: 25413004]
4. Caulfield MP, Birdsall NJ. International Union of Pharmacology. XVII. Classification of Muscarinic Acetylcholine Receptors. *Pharmacol Rev.* 1998; 50:279–290. [PubMed: 9647869]
5. Karakiulakis G, Roth M. Muscarinic Receptors and Their Antagonists in Copd: Anti-Inflammatory and Antiremodeling Effects. *Mediators Inflammation.* 2012; 2012:409580.
6. Dale PR, Cernecka H, Schmidt M, Dowling MR, Charlton SJ, Pieper MP, Michel MC. The Pharmacological Rationale for Combining Muscarinic Receptor Antagonists and Beta-Adrenoceptor Agonists in the Treatment of Airway and Bladder Disease. *Curr Opin Pharmacol.* 2014; 16:31–42. [PubMed: 24682092]
7. Levey AI. Muscarinic Acetylcholine Receptor Expression in Memory Circuits: Implications for Treatment of Alzheimer Disease. *Proc Natl Acad Sci U S A.* 1996; 93:13541–13546. [PubMed: 8942969]
8. Broadley KJ, Kelly DR. Muscarinic Receptor Agonists and Antagonists. *Recent Res Dev Org Chem.* 2002; 6:747–792.
9. Ruiz de Azua I, Gautam D, Guettier JM, Wess J. Novel Insights into the Function of Beta-Cell M3Muscarinic Acetylcholine Receptors: Therapeutic Implications. *Trends Endocrinol Metab.* 2011; 22:74–80. [PubMed: 21106385]
10. Pieper MP. The Non-Neuronal Cholinergic System as Novel Drug Target in the Airways. *Life Sci.* 2012; 91:1113–1118. [PubMed: 22982180]

11. Nathanson NM. Molecular Properties of the Muscarinic Acetylcholine Receptor. *Annu Rev Neurosci.* 1987; 10:195–236. [PubMed: 2436543]
12. Caulfield MP. Muscarinic Receptors—Characterization, Coupling and Function. *Pharmacol Ther.* 1993; 58:319–379. [PubMed: 7504306]
13. Peralta EG, Ashkenazi A, Winslow JW, Ramachandran J, Capon DJ. Differential Regulation of Pi Hydrolysis and Adenylyl Cyclase by Muscarinic Receptor Subtypes. *Nature.* 1988; 334:434–437. [PubMed: 2841607]
14. Richards MH. Pharmacology and Second Messenger Interactions of Cloned Muscarinic Receptors. *Biochem Pharmacol.* 1991; 42:1645–1653. [PubMed: 1930292]
15. Kruse AC, Ring AM, Manglik A, Hu J, Hu K, Eitel K, Huebner H, Pardon E, Valant C, Sexton PM, Christopoulos A, Felder CC, Gmeiner P, Steyaert J, Weis WI, Garcia KC, Wess J, Kobilka BK. Activation and Allosteric Modulation of a Muscarinic Acetylcholine Receptor. *Nature.* 2013; 504:101–106. [PubMed: 24256733]
16. Ballesteros, JA., Weinstein, H. Integrated Methods for the Construction of Three-Dimensional Models and Computational Probing of Structure–Function Relations in G Protein-Coupled Receptors. In: Stuart, CS., editor. *Methods in Neurosciences.* Vol. 25. Academic Press; New York: 1995. p. 366-428.
17. Haga K, Kruse AC, Asada H, Yurugi-Kobayashi T, Shiroishi M, Zhang C, Weis WI, Okada T, Kobilka BK, Haga T, Kobayashi T. Structure of the Human M2Muscarinic Acetylcholine Receptor Bound to an Antagonist. *Nature.* 2012; 482:547–551. [PubMed: 22278061]
18. Gallagher K, Sharp K. Electrostatic Contributions to Heat Capacity Changes of DNA-Ligand Binding. *Biophys J.* 1998; 75:769–776. [PubMed: 9675178]
19. Sharp KA. Polyelectrolyte Electrostatics: Salt Dependence, Entropic, and Enthalpic Contributions to Free Energy in the Nonlinear Poisson–Boltzmann Model. *Biopolymers.* 1995; 36:227–243.
20. Chambers CC, Hawkins GD, Cramer CJ, Truhlar DG. Model for Aqueous Solvation Based on Class Iv Atomic Charges and First Solvation Shell Effects. *J Phys Chem.* 1996; 100:16385–16398.
21. Li J, Zhu T, Cramer CJ, Truhlar DG. New Class Iv Charge Model for Extracting Accurate Partial Charges from Wave Functions. *J Phys Chem A.* 1998; 102(10):1820–1831.
22. Huebner H, Schellhorn T, Gienger M, Schaab C, Kaindl J, Leeb L, Clark T, Moeller D, Gmeiner P. Structure-Guided Development of Heterodimer-Selective GPCR Ligands. *Nat Commun.* 2016; 7:12298. [PubMed: 27457610]
23. Huebner H, Haubmann C, Utz W, Gmeiner P. Conjugated Enynes as Nonaromatic Catechol Bioisosteres: Synthesis, Binding Experiments, and Computational Studies of Novel Dopamine Receptor Agonists Recognizing Preferentially the D(3) Subtype. *J Med Chem.* 2000; 43:756–762. [PubMed: 10691700]
24. Conklin BR, Farfel Z, Lustig KD, Julius D, Bourne HR. Substitution of Three Amino Acids Switches Receptor Specificity of Gq Alpha to That of Gi Alpha. *Nature.* 1993; 363:274–276. [PubMed: 8387644]
25. Kruse AC, Kobilka BK, Gautam D, Sexton PM, Christopoulos A, Wess J. Muscarinic Acetylcholine Receptors: Novel Opportunities for Drug Development. *Nat Rev Drug Discovery.* 2014; 13:549–560. [PubMed: 24903776]
26. Sterling T, Irwin JJ. Zinc 15 - Ligand Discovery for Everyone. *J Chem Inf Model.* 2015; 55:2324–2337. [PubMed: 26479676]
27. Irwin JJ, Shoichet BK. Zinc—a Free Database of Commercially Available Compounds for Virtual Screening. *J Chem Inf Model.* 2005; 45:177–182. [PubMed: 15667143]
28. Mysinger MM, Shoichet BK. Rapid Context-Dependent Ligand Desolvation in Molecular Docking. *J Chem Inf Model.* 2010; 50:1561–1573. [PubMed: 20735049]
29. Shoichet BK, Kuntz ID. Matching Chemistry and Shape in Molecular Docking. *Protein Eng, Des Sel.* 1993; 6:723–732.
30. Gilson MK, Honig BH. Calculation of Electrostatic Potentials in an Enzyme Active Site. *Nature.* 1987; 330:84–86. [PubMed: 3313058]
31. Meng EC, Shoichet BK, Kuntz ID. Automated Docking with Grid-Based Energy Evaluation. *J Comput Chem.* 1992; 13:505–524.

32. Lin H, Sassano MF, Roth BL, Shoichet BK. A Pharmacological Organization of G Protein-Coupled Receptors. *Nat Methods*. 2013; 10:140–146. [PubMed: 23291723]
33. O'Meara MJ, Ballouz S, Shoichet BK, Gillis J. Ligand Similarity Complements Sequence, Physical Interaction, and Co-Expression for Gene Function Prediction. *PLoS One*. 2016; 11:e0160098. [PubMed: 27467773]
34. Manglik A, Lin H, Aryal DK, McCorvy JD, Dengler D, Corder G, Levit A, Kling RC, Bernat V, Huebner H, Huang XP, Sassano MF, Giguere PM, Loeber S, Da D, Scherrer G, Kobilka BK, Gmeiner P, Roth BL, Shoichet BK. Structure-Based Discovery of Opioid Analgesics with Reduced Side Effects. *Nature*. 2016; 537:185–190. [PubMed: 27533032]
35. Huang XP, Karpiak J, Kroeze WK, Zhu H, Chen X, Moy SS, Sadoris KA, Nikolova VD, Farrell MS, Wang S, Mangano TJ, Deshpande DA, Jiang A, Penn RB, Jin J, Koller BH, Kenakin T, Shoichet BK, Roth BL. Allosteric Ligands for the Pharmacologically Dark Receptors Gpr68 and Gpr65. *Nature*. 2015; 527:477–483. [PubMed: 26550826]
36. Powers RA, Morandi F, Shoichet BK. Structure-Based Discovery of a Novel, Noncovalent Inhibitor of Ampc Beta-Lactamase. *Structure*. 2002; 10:1013–1023. [PubMed: 12121656]
37. Carlsson J, Yoo L, Gao ZG, Irwin JJ, Shoichet BK, Jacobson KA. Structure-Based Discovery of A2a Adenosine Receptor Ligands. *J Med Chem*. 2010; 53:3748–3755. [PubMed: 20405927]
38. Bookout, AL., Cummins, CL., Mangelsdorf, DJ., Pesola, JM., Kramer, MF. *Current Protocols in Molecular Biology*. John Wiley & Sons; Hoboken, NJ: 2006. High-Throughput Real-Time Quantitative Reverse Transcription PCR. doi:15.8.110.1002/0471142727.mb1508s73
39. Davies M, Nowotka M, Papadatos G, Dedman N, Gaulton A, Atkinson F, Bellis L, Overington JP. ChEMBL Web Services: Streamlining Access to Drug Discovery Data and Utilities. *Nucleic Acids Res*. 2015; 43:W612–620. [PubMed: 25883136]
40. Gaulton A, Hersey A, Nowotka M, Bento AP, Chambers J, Mendez D, Mutowo P, Atkinson F, Bellis LJ, Cibrian-Uhalte E, Davies M, Dedman N, Karlsson A, Magarinos MP, Overington JP, Papadatos G, Smit I, Leach AR. The ChEMBL Database in 2017. *Nucleic Acids Res*. 2017; 45:D945–D954. [PubMed: 27899562]
41. Gaulton A, Bellis LJ, Bento AP, Chambers J, Davies M, Hersey A, Light Y, McGlinchey S, Michalovich D, Al-Lazikani B, Overington JP. ChEMBL: A Large-Scale Bioactivity Database for Drug Discovery. *Nucleic Acids Res*. 2012; 40:D1100–1107. [PubMed: 21948594]
42. Law V, Knox C, Djoumbou Y, Jewison T, Guo AC, Liu Y, Maciejewski A, Arndt D, Wilson M, Neveu V, Tang A, Gabriel G, Ly C, Adamjee S, Dame ZT, Han B, Zhou Y, Wishart DS. Drugbank 4.0: Shedding New Light on Drug Metabolism. *Nucleic Acids Res*. 2014; 42:D1091–1097. [PubMed: 24203711]
43. Rogers DJ, Tanimoto TT. A Computer Program for Classifying Plants. *Science*. 1960; 132:1115–1118. [PubMed: 17790723]
44. Tschammer N, Elsner J, Goetz A, Ehrlich K, Schuster S, Ruberg M, Kuehhorn J, Thompson D, Whistler J, Huebner H, Gmeiner P. Highly Potent 5-Aminotetrahydropyrazolopyridines: Enantioselective Dopamine D3 Receptor Binding, Functional Selectivity, and Analysis of Receptor-Ligand Interactions. *J Med Chem*. 2011; 54:2477–2491. [PubMed: 21388142]
45. Moeller D, Banerjee A, Uzuneser TC, Skultety M, Huth T, Plouffe B, Huebner H, Alzheimer C, Friedland K, Mueller CP, Bouvier M, Gmeiner P. Discovery of G Protein-Biased Dopaminergics with a Pyrazolo[1:5-a]Pyridine Substructure. *J Med Chem*. 2017; 60:2908–2929. [PubMed: 28248104]
46. Lowry OH, Rosebrough NJ, Farr AL, Randall RJ. Protein Measurement with the Folin Phenol Reagent. *J Biol Chem*. 1951; 193:265–275. [PubMed: 14907713]
47. Mathiesen JM, Vedel L, Brauner-Osborne H. Camp Biosensors Applied in Molecular Pharmacological Studies of G Protein-Coupled Receptors. *Methods Enzymol*. 2013; 522:191–207. [PubMed: 23374187]
48. Valant C, Gregory KJ, Hall NE, Scammells PJ, Lew MJ, Sexton PM, Christopoulos A. A Novel Mechanism of G Protein-Coupled Receptor Functional Selectivity. Muscarinic Partial Agonist Mcn-a-343 as a Bitopic Orthosteric/Allosteric Ligand. *J Biol Chem*. 2008; 283:29312–29321. [PubMed: 18723515]

49. Gopalakrishnan M, Monteggia LM, Anderson DJ, Molinari EJ, Piattoni-Kaplan M, Donnelly-Roberts D, Arneric SP, Sullivan JP. Stable Expression, Pharmacologic Properties and Regulation of the Human Neuronal Nicotinic Acetylcholine Alpha 4 Beta 2 Receptor. *J Pharmacol Exp Ther.* 1996; 276:289–297. [PubMed: 8558445]
50. Cheng YC, Prusoff WH. Relationship between the Inhibition Constant (K_i) and the Concentration of Inhibitor Which Causes 50 Per Cent Inhibition (I_{50}) of an Enzymatic Reaction. *Biochem Pharmacol.* 1973; 22:3099–3108. [PubMed: 4202581]

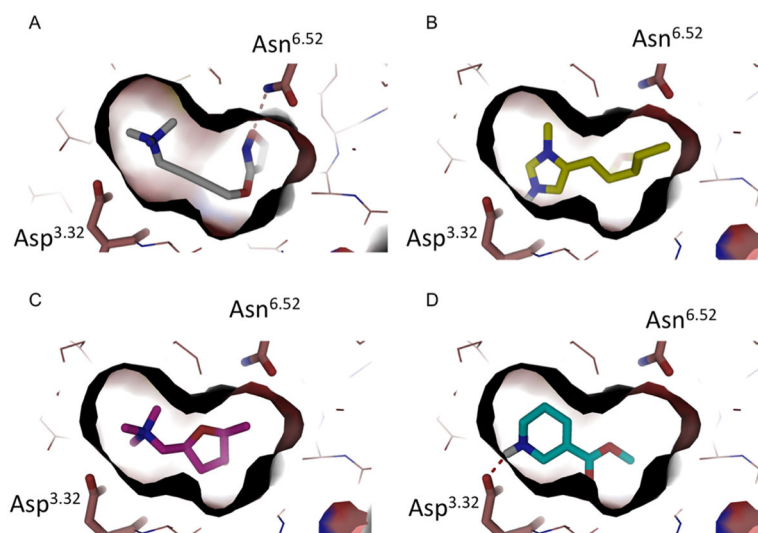


Figure 1. (A) The crystal structure of M₂ active state in a complex with iperoxo (PDB 4MQS). Residues Asn^{6.52} and Asp^{3.32} are represented as sticks and hydrogen bonds as red broken lines. Iperoxo fits tightly in the binding site. (B–D) Docking poses of pilocarpine (B), muscarine (C), and arecoline (D) in the M₂ active state structure.

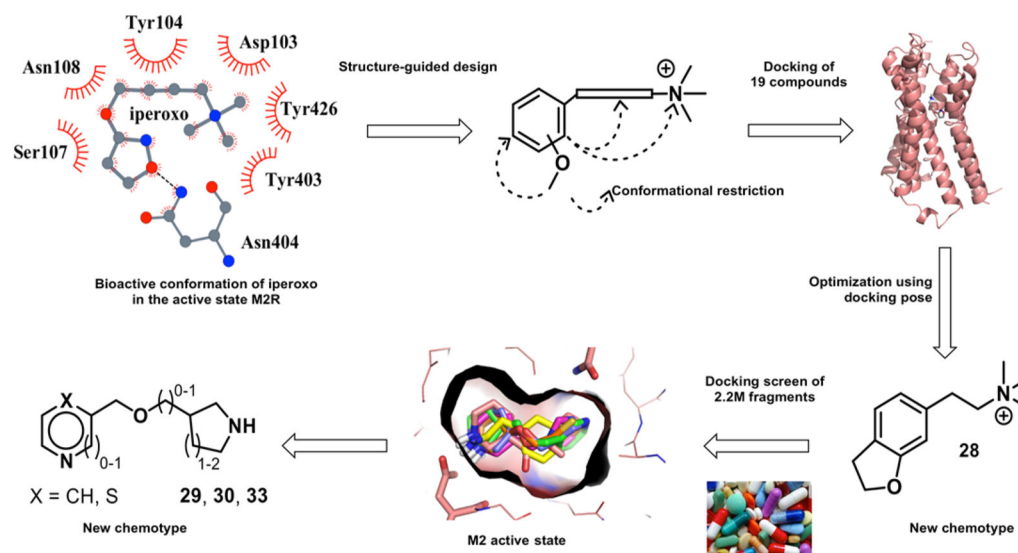


Figure 2. Structure-based discovery of new muscarinic agonists: project flow. Structure-guided design from the M₂R/iperoxo complex (top left) led to 19 candidate ligands chemically distinct from previous agonists. Optimization led to the improved compound **28**, a new agonist scaffold (bottom right). A docking screen of a large fragment library (bottom middle) led to three still newer agonists (bottom left).

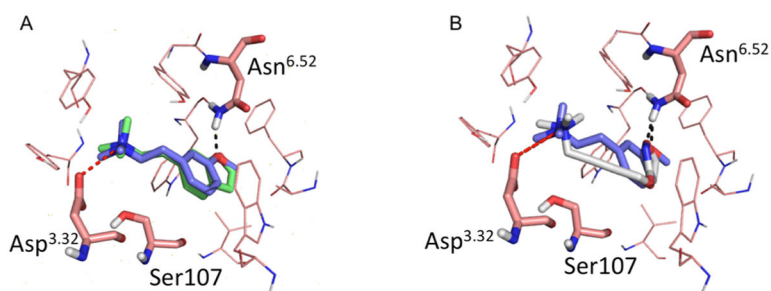


Figure 3.

(A) Superposition of compound **17** (green) and compound **3** (purple). Residues Asn^{6.52}, Asp^{3.32}, and Ser107 are represented as sticks. Both compounds hydrogen bond (black broken lines) with Asn^{6.52}. (B) Superposition between the iperoxo (silver) pose in the M₂R active state structure (PDB 4MQS¹⁵) and the docked pose of compound **3** (purple). Both compounds appear to hydrogen bond with Asn^{6.52}, ion pair with Asp^{3.32}, and are enclosed by an aromatic cage composed of Tyr104, Tyr403, and Tyr426.

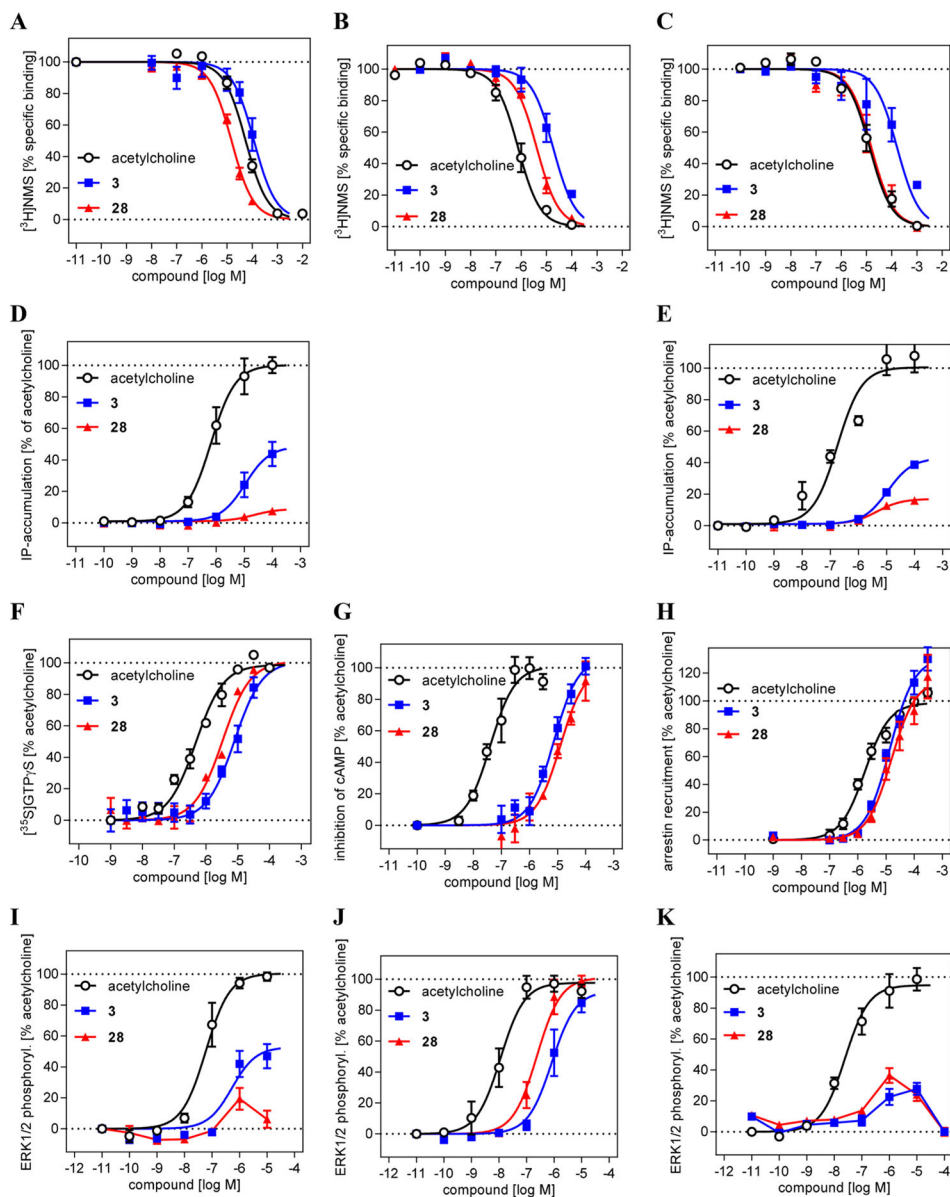


Figure 4.

Detailed investigation of the new muscarinic agonists **3** and **28**. (A–C) Binding behavior at whole cells expressing the muscarinic receptor subtypes M₁ (A), M₂ (B), and M₃ (C) in comparison to the natural ligand acetylcholine. (D–G) M₂ selective signaling of **28** indicated by a weak activation of M₁ and M₃ stimulated IP accumulation (D and E, respectively) and full agonist effect in M₂ mediated GTPγS binding (F) and inhibition of cAMP accumulation (G). (H) M₂ mediated β-arrestin recruitment displays full agonist effect for **28**. (I–K) Downstream signaling shows M₂ selective agonist properties for **28** as determined in a ERK1/2 phosphorylation assay for M₁ (I), M₂ (J), and M₃ (K).

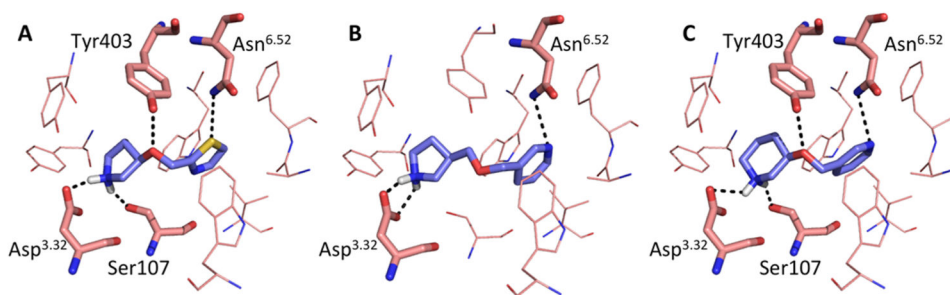
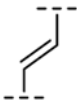


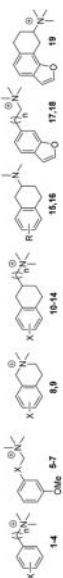


Figure 5. Docking poses of compounds **29** (A), **30** (B), and **33** (C) in the M₂R active state structure (PDB 4MQS). Residues Asn^{6.52}, Asp^{3.32}, Ser107, and Tyr403 are represented as sticks. Hydrogen bonds are represented in black.

Table 1

Activities and Structural Complementarity of Compounds 1–19 to the M₁R, M₂R, and M₃R Receptor Subtypes (K_i in μ M)

compound	X	n	K_i (μ M) ^d			IP accumulation assay ^b			docking	
			M ₁ R	M ₂ R	M ₃ R	EC ₅₀ [μ M] ^c	E _{max} [%] ^d	docking score active state	H-bond to Asn ⁶⁵²	predicted agonist?
1	2-OMe	1	26±15	>50	>50	18±3.3	51±15	-8.13	N	-
2	2-OMe	2	4.9±1.1	5.7±2.3	4.7±1.2	9.1±3.9	21±7.8	-27.11	N	-
3	3-OMe	2	33±6.6	14±6.1	>50	12±2.8	75±7.5	-32.89	Y	+
4	3-OMe	3	0.33±0.073	0.63±0.17	0.62±0.20	/	<10 ^e	-15.56	N	-
5		-	16±0.88	22±2.6	21±4.5	/	/	3.86	N	-
6		-	20±4.9	50±25	20±5.9	/	/	24.43	N	-
7		-	7.3±1.1	15±2.5	8.7±4.4	/	/	81.61/5.74/9.66/15.82 ^h	N/N/Y/Y	-
8	5-OMe	-	14±3.6	26±14	24±9.4	/	/	-18.61	N	-
9	8-OMe	-	17±8.5	6.3±2.3	5.8±2.2	/	/	-10.97	N	-
10	8-OMe	0	1.0±0.19	0.93±0.15	2.0±0.53	/	/	79.83/33.04 ^h	N	-
11	8-OH	0	2.9±1.1	4.2±2.5	16±3.5	/	/	-4.32/7.83 ^h	Y	-
12	8-OMe	1	1.8±0.35	1.3±0.18	3.9±0.26	/	/	28.12/-6.16 ^h	Y	-
13	5-OMe	0	2.5±0.35	4.4±2.2	4.0±0.42	/	/	93.73/89.59 ^h	Y	-
14	5-OMe	1	17±8.5 ^f	14±8.9 ^f	25±2.8 ^f	/	/	14.86/11.16 ^h	N/Y	-
15	8-OMe	0	2.0±1.5 ^f	1.2±0.88 ^f	0.83±0.22 ^f	/	/	74.55/34.28 ^h	Y/N	-
16	8-OH	0	>50 ^f	>50 ^f	28±13 ^f	/	/	-6.56/6.86 ^h	Y/Y	-
17	-	1	0.023±0.0053	0.14±0.049	0.041±0.011	0.22±0.21	-14±18	-27.79	Y	+



compound	K_i (μM) ^d				IP accumulation assay ^b			docking	
	M_1R	M_2R	M_3R	EC_{50} [μM] ^c	E_{max} [%] ^d	docking score	active state	H-bond to Asn ^{6.52}	predicted agonist?
18	-	0.063±0.012	0.23±0.028	0.14±0.053	0.027±0.022	12±13	-15.49	Y	-
19	-	0.38±0.063	0.79±0.17	0.69±0.090	2.3±1.9	-8.3±8.0	39.28/28.65 ^h	N/N	-
ipetroxo		350±50 ^g	4.9±0.60 ^g	550±73 ^g	0.28±0.088 ^g	125±2.3	NA	Y	NA
acetylcholine		5.8±1.5	0.39±0.084	4.7±1.3	0.056±28	92±5.5	-28.22	Y	+
carbachol		63±12	4.1±1.1	51±12	0.89±0.22	100	-32.23	Y	+

^a K_i values ± SEM derived from 3–8 individual competition binding experiments using the radioligand [³H]N-methyl-scopolamine bromide and membranes from HEK cells transiently expressing the human M_1R , M_2R or M_3R .

^b Second, less sensitive IP accumulation assay with COS cells coexpressing M_2R and $G\alpha_{q15}HA$.

^c EC_{50} values ± SEM from 3–8 individual experiments each done in triplicate.

^d E_{max} values relative to the full effect of carbachol.

^e E_{max} at 10 μM (no complete dose–response curve was available).

^f K_i values ± SD derived from two independent competition binding experiments.

^g Values are displayed in nM ± SEM.

^h Racemic mixture. “/” = not determined

Screening of the Second Set Compounds 20–28 (Receptor Binding Affinities to M₁, M₂, and M₃ (K_i in μ M), M₂ Receptor Activation and Docking Data)

Table 2

compd	R ¹	R ²	X	K _i [μ M] ^e			IP accumulation assay ^b			docking		
				M ₁ R	M ₂ R	M ₃ R	EC ₅₀ [μ M] ^c	E _{max} [%] ^d	docking score	active state	H-bond to Asn ⁶⁵²	predicted agonist?
20				0.74 ± 0.13	1.0 ± 0.25	0.78 ± 0.10	8.2 ± 5.5	-12 ± 1.5	-40.99	Y	+	
21	OH	H	H,H	20 ± 11	14 ± 4.7	13 ± 4.8	10 ± 4.1	44 ± 10	-36.29	Y	+	
22	OMe	F	H,H	7.1 ± 2.5	0.98 ± 0.61	14 ± 5.9	23 ± 10	44 ± 4.7	-29.73	Y	+	
23	OMe	H	H,OH	13 ± 5.5	29 ± 8.7	12 ± 4.2		<10 ^e	-32.23/-30.97 ^g	Y/N	+/-	
24	OMe	H	O	0.17 ± 0.014 ^f	2.4 ± 0.42 ^f	0.21 ± 0.028 ^f		<10 ^e	-34.56	Y	+	
25	OEt	H	H,H	42 ± 14	27 ± 9.9	43 ± 10		40 ^e	-23.00	Y	+	
26	Cl	H	H,H	4.5 ± 1.1	4.8 ± 1.4	5.8 ± 1.8		<10 ^e	-39.07	N	-	
27	OCF ₃	H	H,H	7.8 ± 1.6	9.2 ± 2.1	11 ± 6.6		<10 ^e	-28.6	Y	+	
28				6.4 ± 0.96	13 ± 3.3	6.3 ± 1.7	21 ± 7.6	62 ± 6.6	-23.47	Y	+	

^a K_i values ± SEM derived from three to eight individual competition binding experiments using the radioligand [³H]N-methyl-scopolamine bromide.^b Second, less sensitive IP accumulation assay with COS cells coexpressing M₂R and G α qi5HA.^c EC₅₀ values ± SEM from three individual experiments each done in triplicate.^d E_{max} values ± SEM relative to the full effect of carbachol.^e Maximum effect at 100 μ M; no complete dose-response curve could be determined.^f K_i values ± SD derived from 2 individual competition binding experiments.^g Racemic mixture.

Table 3

Signaling Selectivity of New Muscarinic Agonists 3 and 28 vs Acetylcholine

test system	test compounds				
	receptor subtype	acetylcholine	3	28	
whole cell binding ^a	pK_i [M]/ K_i [μ M]	4.64 ± 0.04/23	4.28 ± 0.09/52	5.17 ± 0.03/6.8	
	pK_i [M]/ K_i [μ M]	6.42 ± 0.06/0.38	5.04 ± 0.08/9.1	5.69 ± 0.07/2.0	
	pK_i [M]/ K_i [μ M]	5.17 ± 0.07/6.8	4.09 ± 0.15/81	5.11 ± 0.10/7.8	
IP accumulation ^b	pEC_{50} [M]/ EC_{50} [μ M]	6.21 ± 0.11/0.62	5.04 ± 0.17/9.1	5.32 ± 0.33/4.8	
	E_{max} [% ± SEM] ^c	100	48 ± 5	8 ± 2	
GTP γ S binding ^d	pEC_{50} [M]/ EC_{50} [μ M]	M ₂ R			
	pEC_{50} [M]/ EC_{50} [μ M]	M ₃ R	4.98 ± 0.07/10	5.43 ± 0.23/3.7	
	E_{max} [% ± SEM] ^c	100	43 ± 2	17 ± 2	
	pEC_{50} [M]/ EC_{50} [μ M]	M ₁ R			
	pEC_{50} [M]/ EC_{50} [μ M]	M ₂ R	6.29 ± 0.07/0.51	5.11 ± 0.06/7.8	5.48 ± 0.07/3.3
inhibition of cAMP accumulation ^e	E_{max} [% ± SEM] ^c	100	100	100	
	pEC_{50} [M]/ EC_{50} [μ M]	M ₃ R			
	pEC_{50} [M]/ EC_{50} [μ M]	M ₁ R			
	pEC_{50} [M]/ EC_{50} [μ M]	M ₂ R	7.31 ± 0.19/0.049	5.20 ± 0.18/6.3	4.96 ± 0.13/11
	E_{max} [%] ^c	100	108 ± 9	102 ± 16	
β -arrestin recruitment ^f	pEC_{50} [M]/ EC_{50} [μ M]	M ₃ R			
	pEC_{50} [M]/ EC_{50} [μ M]	M ₁ R			
	pEC_{50} [M]/ EC_{50} [μ M]	M ₂ R	5.72 ± 0.09/1.9	4.85 ± 0.05/14	4.76 ± 0.11/17
	E_{max} [%] ^c	100	133 ± 7	118 ± 9	
	pEC_{50} [M]/ EC_{50} [μ M]	M ₃ R			
ERK1/2 phosphorylation ^g	pEC_{50} [M]/ EC_{50} [μ M]	M ₁ R	7.33 ± 0.15/0.047	6.27 ± 0.23/0.54	na ^h
	E_{max} [%] ^c	100	53 ± 6		
	pEC_{50} [M]/ EC_{50} [μ M]	M ₂ R	7.90 ± 0.08/0.013	6.08 ± 0.14/0.83	6.62 ± 0.11/0.24
	E_{max} [%] ^c	100	92 ± 8	~100	

test system	test compounds		receptor subtype	acetylcholine	pEC ₅₀ [M]/EC ₅₀ [μ M]	E _{max} [%] ^c
	3	28				
	na ^b	na ^b	M ₃ R	7.64 ± 0.08/0.023	100	

^a Affinity to M₁R, M₂R, or M₃R from whole cell receptor binding performed with CHO cells stably expressing a given receptor subtype and with the antagonist radioligand [³H]N-methyl scopolamine; pK_i ± SEM values are the means of 4–6 individual experiments each in duplicate.

^b Gq-protein mediated functional activity was measured with the same cells using the IP-One assay (Cisbio); pEC₅₀ ± SEM values are the means of 3–4 individual experiments each in duplicate.

^c Maximum efficacy vs acetylcholine.

^d Gi/o-Protein activation was measured using [³⁵S]GTP- γ S binding with membranes from the same cells stably expressing M₂R; pEC₅₀ ± SEM values are mean values from three individual experiments each in duplicate.

^e Inhibition of cAMP accumulation was done with HEK cells stably expressing the Epac cAMP sensor and M₂R; pEC₅₀ ± SEM were means of 4–5 individual experiments each in duplicate.

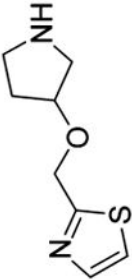

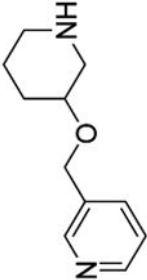
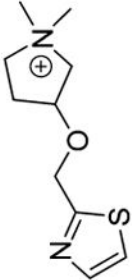
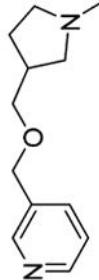
^f β -Arrestin recruitment assay was performed with HEK cells stably expressing the β -arrestin-TEVprotease and transiently transfected with M2-TEV-TTA; pEC₅₀ ± SEM values are the means of 4–5 individual experiments, each in triplicate.

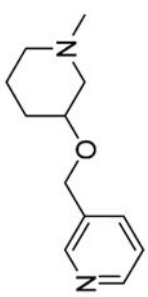
^g ERK1/2 phosphorylation was measured by AlphaScreen with CHO cells stably expressing M₁R, M₂R, or M₃R; pEC₅₀ ± SEM values are the means of 3–4 individual experiments, each in duplicate.

^h na: could not be estimated.

Table 4

Experimentally Active Molecules from Docking and Their Synthesized Analogues

compound		K_i [μM] ^d				IP accumulation assay ^b		docking	
Rank	Structure	M ₁	M ₂	M ₃	EC ₅₀ [μM] ^c	E _{max} [%] ^d	Tc to closest muscarinic ligand	ZINC IDs of closest muscarinic ligand ^e	
29		4.2±0.65	6.0±2.5	4.1±1.6	9.9±1.7	74±4.6	0.20	C13739835	
30		18±9.7	11±2.0	36±6.7	29±13	74±14	0.34	C34802190	
33		10±2.9	17±4.9	10±2.8	13±4.8	60±6.5	0.33	C27984351	
29a		6.1±1.8	10±1.1	12±1.4	10±4.3	28±1.2	0.28	C00000346	
30a		38±16	39±4.4	75±6.4	>100	38±4.8 ^f	0.33	C34802190	

compound		K_i [μM] ^a				IP accumulation assay ^b			docking	
Rank	Structure	M ₁	M ₂	M ₃	EC ₅₀ [μM] ^c	E _{max} [%] ^d	Tc to closest muscarinic ligand	ZINC IDs of closest muscarinic ligand ^e		
33a		20±3.2	46±2.0	42±2.2	50±7.4	33±10	0.31	C27984351		

^a K_i values ± SEM derived from 3–8 individual competition binding experiments using the radioligand [³H]N-methyl-scopolamine bromide.

^b Second, less sensitive IP accumulation assay with COS cells coexpressing M₂R and Gαq15HA.

^c EC₅₀ values ± SEM from 4–6 individual experiments each done in triplicate.

^d E_{max} values ± SEM relative to the full effect of carbachol.

^e 2D structures are presented in Supporting Information, Table S4.

^f Maximum effect at 100 μM ; no complete dose–response curve could be determined.